

This discussion paper is/has been under review for the journal *Atmospheric Chemistry and Physics (ACP)*. Please refer to the corresponding final paper in *ACP* if available.

Initial fate of fine ash

U. Niemeier et al.

Initial fate of fine ash and sulfur from large volcanic eruptions

U. Niemeier¹, C. Timmreck¹, H.-F. Graf², S. Kinne¹, S. Rast¹, and S. Self³

¹Max Planck Institute for Meteorology, Bundesstr. 53, 20146 Hamburg, Germany

²University of Cambridge, Centre for Atmospheric Science, Downing Place, Cambridge, CB2 3EN, UK

³Department of Earth Science, Open University, Milton Keynes, MK7 6AA, UK

Received: 8 June 2009 – Accepted: 24 July 2009 – Published: 24 August 2009

Correspondence to: U. Niemeier (ulrike.niemeier@zmaw.de)

Published by Copernicus Publications on behalf of the European Geosciences Union.

Title Page

Abstract

Introduction

Conclusions

References

Tables

Figures

◀

▶

◀

▶

Back

Close

Full Screen / Esc

Printer-friendly Version

Interactive Discussion



Abstract

Large volcanic eruptions emit huge amounts of sulfur and fine ash into the stratosphere. These products cause an impact on radiative processes, temperature and wind patterns. In simulations with a General Circulation Model including detailed aerosol microphysics, the relation between the impact of sulfur and fine ash is determined for different eruption strengths and locations, one in the tropics and one in high Northern latitudes. Fine ash with effective radii between $1\ \mu\text{m}$ and $15\ \mu\text{m}$ has a lifetime of several days only. Nevertheless, the strong absorption of shortwave and longwave radiation causes additional heating and cooling of $\pm 20\ \text{K/day}$ and impacts the evolution of the volcanic cloud. Depending on the location of the volcanic eruption, transport direction changes due to the presence of fine ash, vortices develop and temperature anomalies at ground increase. The results show substantial impact on the local scale but only minor impact on the evolution of sulfate in the stratosphere in the month after the simulated eruptions.

1 Introduction

Volcanic aerosols are an active component of the climate system and play multiple roles in physical and biogeochemical exchanges between the atmosphere, land surface and ocean. The impact of sulfuric aerosols on climate after a volcanic eruption has been comprehensively studied, but in General Circulation models (GCMs) mainly aerosol bulk models assuming a fixed aerosol partition (Oman et al., 2006; Timmreck et al., 1999, 2003) or a prescribed aerosol distribution e.g. (Stenchikov et al., 1998; Kirchner et al., 1999; Thomas et al., 2009) was used so far. The simulations presented here are different to previous GCM studies because they include detailed aerosol microphysics, calculating the nucleation and accumulation processes as well as the aerosol size distribution in detail.

ACPD

9, 17531–17577, 2009

Initial fate of fine ash

U. Niemeier et al.

Title Page

Abstract

Introduction

Conclusions

References

Tables

Figures

◀

▶

◀

▶

Back

Close

Full Screen / Esc

Printer-friendly Version

Interactive Discussion



Initial fate of fine ash

U. Niemeier et al.

[Title Page](#)[Abstract](#)[Introduction](#)[Conclusions](#)[References](#)[Tables](#)[Figures](#)[◀](#)[▶](#)[◀](#)[▶](#)[Back](#)[Close](#)[Full Screen / Esc](#)[Printer-friendly Version](#)[Interactive Discussion](#)

The impact of volcanic eruptive products on climate strongly depends on eruption strength and height of the resulting plume. An eruption has a long (month to years) climatic influence when the ash and SO₂ cloud reaches the stratosphere. In the troposphere the eruption products are quickly sedimented and washed out. Only in the stratosphere they can be dispersed over long distances. Additionally, the influence of the volcanic eruption depends on the location. Volcanos in the tropics have a global effect and high latitude volcanos show a more regional to hemispheric effect.

Little attention has been paid to the impact of fine ash on climate and biogeochemical processes. Volcanic ash is composed of silicate (including glass and sometimes mineral components) that scatters and absorbs infrared light differently from water and ice in the atmosphere. Fine ash can be globally transported and change chemistry, cloudiness and radiation budget of the atmosphere for a few weeks. The 15 June 1991 climactic eruption of Mt. Pinatubo for example, covered an area of approximately 4×10^5 km² with a minimum of 1mm ash on Luzon Island and across the South China Sea (Wiesner et al., 2004). Over the ash-covered areas the surface albedo and hydrology are changed significantly with consequences on local and potentially global climate (Jones et al., 2007). Agriculture and biosphere are heavily affected by ash deposits. A layer of volcanic ash one centimetre thick disrupt most forms of agriculture for more than a growing season, and lesser amounts (a few millimetres) can destroy many kinds of crops (e.g. Self, 2006). Furthermore, changes in soil composition can be expected.

Deposition of volcanic ash may provide an external nutrient source for primary production in ocean surface waters, in particular through iron fertilisation (Duggen et al., 2007). This effect is strongest in high-nutrient but low-productivity (low-iron) areas in the Pacific and the Southern Ocean. Surrounded by active volcanoes, in these areas the fallout of ash can have a high potential to induce globally significant, transient net CO₂ removal from the upper ocean and hence from the atmosphere.

During the past years, it has been possible to detect fine ash by satellite instruments (e.g. Prata and Kerkmann, 2007; Guo et al., 2004). This is extremely helpful for aviation safety, as fine ash is a source of danger, which in low concentration can not be seen by

the pilots of an air plane (Tupper et al., 2004). The transport of ash has been simulated in dispersion models (e.g. PUFF) with prescribed meteorological fields (Searcy et al., 1998; Fero et al., 2008). Folch et al. (2008) coupled an ash dispersion model to the Weather research and Forecasting model (WRF), allowing also to forecast the dispersion of ash. These studies were not concerned with the interaction of the ash cloud to radiative processes, thus neglecting the interaction between cloud and meteorological processes. On the other hand, the Active Tracer High Resolution Atmospheric Model ATHAM (Textor et al., 2006; Herzog et al., 1998) and the 3-D simulation by Suzuki and Koyaguchi (2009) show detailed information on the processes in the eruption cloud on the local scale in the very first phase, i.e. few hours, of the eruption.

This paper determines the impact of fine ash, emitted into the stratosphere by large volcanic eruptions (5 km³ erupted material and above), on meteorological processes and tracer transport on the global scale for several days. Even though ash has a short atmospheric lifetime, the indirect effect of changing wind patterns caused by the radiative impact of ash, influences other tracers like sulfate with potentially global effects. To calculate these indirect impacts, radiative parameters of ash are taken into account, the size of the ash particles changes with time and sedimentation and deposition are included as sink processes. For these studies the global general circulation model MAECHAM5 was used including the interactively coupled aerosol microphysics model HAM. By comparison with other observations, we show the capability of MAECHAM5-HAM to simulate the evolution of a volcanic cloud consisting of ash and sulfate (Sect. 4). Thereafter the impact of ash on meteorological processes is investigated for two simulated volcanic eruptions, one in the tropics and one at high latitudes (Sect. 5). We will show the direct impact of ash during the first four weeks after the eruption on heating rates and temperatures and determine a possible longer lasting indirect impact on the lifetime of sulfate depending on location and emission strength.

Initial fate of fine ash

U. Niemeier et al.

[Title Page](#)[Abstract](#)[Introduction](#)[Conclusions](#)[References](#)[Tables](#)[Figures](#)[◀](#)[▶](#)[◀](#)[▶](#)[Back](#)[Close](#)[Full Screen / Esc](#)[Printer-friendly Version](#)[Interactive Discussion](#)

2 Model description

The study was performed with the general circulation model MAECHAM5 (Giorgetta et al., 2006), a middle atmosphere version of the ECHAM5 model (Roeckner et al., 2003). The model solves prognostic equations for vorticity, divergence, surface pressure and temperature, expressed in terms of spherical harmonics with a triangular truncation. Water vapour, cloud liquid water, cloud ice and trace components are transported with a flux form semi-Lagrangian transport scheme (Lin and Rood, 1996). MAECHAM5 is integrated with a spectral truncation of 42 (T42) and 39 vertical levels up to 0.1 hPa. The integration is performed with a time step of 900 s.

2.1 Fine ash

For this study, a fine ash module was included into MAECHAM5. To calculate the transport and distribution of fine ash, two passive tracers were introduced into the model: ash mass and number concentration. They are transported independently from each other, thus the mean radius of fine ash varies during the simulation.

Sedimentation, wet and dry deposition processes are implemented similar to the processes for dust in the ECHAM5 aerosol microphysics module HAM (Stier et al., 2005). The emitted fine ash is assumed to be non-soluble particulates with a mean radius of $2.4 \mu\text{m}$, an effective radius of $5.7 \mu\text{m}$, and a density of a single fine ash particle of 2400 kg/m^3 . For the log-normal distribution of particle size, a fixed standard deviation $\sigma=1.8$ is assumed.

Optical parameters for fine ash are calculated from the time dependent aerosol mass mixing ratio, normalised extinction and absorption coefficients, and a normalised asymmetry factor. To derive these normalised parameters, dependent on wavelength and size, Mie calculations were performed for all spectral bands of the MAECHAM5 radiation scheme. Therefore, refractive indices for rhyolite were used (Pollack et al., 1973) and the results stored in a look-up table. The look-up table covers effective radii of particles between $0.5 \mu\text{m}$ – $10 \mu\text{m}$.

Initial fate of fine ash

U. Niemeier et al.

Title Page

Abstract

Introduction

Conclusions

References

Tables

Figures



Back

Close

Full Screen / Esc

Printer-friendly Version

Interactive Discussion



2.2 Sulfur

The formation of sulfate aerosol is calculated by the aerosol module HAM (Stier et al., 2005), which is interactively coupled to ECHAM5. The mode setup of M7, the microphysical core of HAM, (Vignati et al., 2004) was changed according to boxmodel studies for large volcanic eruptions (Kokkola et al., 2009). The changes include a new time integration scheme of H₂SO₄ processes, a revised nucleation parameterisation (Vehkamäki, personal communication), a reduction to three modes (nucleation, aitken, accumulation), and a smaller standard deviation for the accumulation mode ($\sigma=1.2$ instead of $\sigma=1.59$). The simulation includes only sulfate aerosol, other aerosols normally used in HAM (e.g. black carbon, organic carbon, sea salt, dust) were ignored. The tropospheric sulfur chemistry is calculated as described in Feichter et al. (1996), and the stratospheric chemistry as in Timmreck et al. (2003). Climatological concentrations of background OH values have been taken from (Timmreck et al., 2003), other gas-phase species from Jöckel et al. (2005).

3 Simulations

We performed an ensemble of five simulations for two different volcanic eruption sites (Table 1): Mt. Pinatubo (15.14° N, 120.35° E) in the tropics and Mt. Katmai, Alaska (58.2° N 155° W) in the northern hemispheric higher latitudes. At each location one simulation always contained SO₂ and fine ash emissions and one SO₂ emissions only. Total volcanic emissions of 17 Mt SO₂ and 100 Mt fine ash, as from Mt. Pinatubo in June 1991 (Read et al., 1993; Krueger et al., 1995), were assumed. To test the influence of eruption strength, a 10 times larger eruption was performed as well. The eruption always started at 1st of June at 06:00 UTC and lasted for 3 h and for 30 h in case with 10 times higher emissions. Thus emissions rate was for both 1.5×10^6 kg (SO₂)/s. To get a more general view on the impact of the fine ash, under varying meteorological conditions, additional single simulations with eruption dates, five days and ten

Initial fate of fine ash

U. Niemeier et al.

Title Page

Abstract

Introduction

Conclusions

References

Tables

Figures

◀

▶

◀

▶

Back

Close

Full Screen / Esc

Printer-friendly Version

Interactive Discussion



days later, were performed. As our focus is on the impact of the fine ash in eruptions at different latitudes, we have chosen the same volcanic strength for both locations to maintain a better comparability. Mt. Katmai can be seen as synonym for any volcano in Southern Alaska. The eruption strength is not related to the real eruption in 1912, when no reliable measurements were available.

SO₂ is injected into the stratosphere into a model layer corresponding to the pressure height level of 30 hPa (~24 km). Satellite observations and ATHAM simulations show that the neutral buoyancy height of ash is lower than that of SO₂ (Schneider et al., 1999; Holasek et al., 1996b). Therefore, fine ash was released at a height of 50 hPa. SO₂ and fine ash each are emitted into one grid box at the latitude and longitude of the volcano. For the initial amount of fine ash emitted into the stratosphere we use an amount commensurate with that emitted by Pinatubo and satellite retrieval data (Guo et al., 2004). We inject a total fine ash particle number of 7.93×10^{22} and a total fine ash mass of 100 Mt over three hours (2.77×10^7 kg/s) into the stratosphere (50 hPa, ~21 km). This corresponds to ca. 1% of the total erupted mass. 66 Mt of the totally emitted fine ash are in the 1 to 15 μm size range of ash particles, comparable to the amount detected by satellite measurements, which suggested 0.6 to 0.9% (Guo et al., 2004) and 0.7 to 0.9% (Wen and Rose, 1994) of the total erupted mass injected into the stratosphere.

4 Comparison to measurements

The eruption of Mt. Pinatubo was the largest one in the last decades (~5 km³ of magma emitted). The processes following in the atmosphere were well documented by observations. We compare our simulation results of detailed aerosol formation and evolution processes to measurements of satellite and lidar instruments. Results in this section base on a single simulation.

Initial fate of fine ash

U. Niemeier et al.

Title Page

Abstract

Introduction

Conclusions

References

Tables

Figures

◀

▶

◀

▶

Back

Close

Full Screen / Esc

Printer-friendly Version

Interactive Discussion



4.1 Fine ash

An effective radius (r_{eff}) of fine ash between 6.2 and 9.33 μm has been retrieved from satellite measurements (Guo et al., 2004) for the first 5 days after the Mt. Pinatubo eruption. ECHAM5-HAM calculates effective radii of 6 μm , quickly decreasing over time to 3 μm . These values are at the lower limit of the satellite retrieval. Figure 1 shows results from the satellite retrieval of HIRS/2 analysed by Guo et al. (2004) after the Mt. Pinatubo eruption and the fine ash mass as calculated in MAECHAM5 for the first days after the eruption. The model gives higher values in the beginning with a quicker decrease of the total fine ash mass and a slower decline after the larger particles are sedimented. After three days r_{eff} is smaller in the model than in the satellite retrievals (Guo et al., 2004) and sedimentation velocity slows down. The ash cloud is dispersed by this time and parts of the cloud with low concentrations might be below the detection limit of the satellite. These areas with lower concentrations are, however, included in the global sum of the simulation results. Hence, we conclude that the simulated fine ash properties agree reasonably well with the observations.

A comparison of the simulated deposition of Mt. Pinatubo fine ash with sediment trap measurements of Wiesner et al. (2004) shows a very similar pattern, even though the passing of Typhoon Yunya¹ was not included in the simulation. This similarity suggests that also larger particles, as found in the sediment traps, reach the stratosphere and are transported with the main stratospheric flow, independent of the Typhoon. The larger particles are not included in the simulation, thus the thickness of the simulated fine ash layer is much smaller as observed.

¹Yunya passed about 75 km northeast of Mt. Pinatubo during the initial stage of the climactic eruption (further details in Wiesner et al., 2004).

Initial fate of fine ash

U. Niemeier et al.

Title Page

Abstract

Introduction

Conclusions

References

Tables

Figures

◀

▶

◀

▶

Back

Close

Full Screen / Esc

Printer-friendly Version

Interactive Discussion



4.2 Sulfate

For a realistic simulation of the volcanic sulfate cloud in the stratosphere, the evolution process of the sulfate and the calculated size of the aerosol is important. To obtain confidence in the simulated evolution of sulfate, we compare the model results over a period of two years to observations. For sulfur, being emitted as SO₂, the assumed climatological OH concentration determines the oxidation rate of SO₂ to H₂SO₄ and the lifetime of SO₂. Sulfate particles are formed by gas to particle transition from H₂SO₄ by condensation, nucleation and coagulation.

Figure 3 shows the rapid decrease of the total global mass of SO₂ after the eruption. The yellow line represents the simulation results, in green and red, results of TOMS and TOVS satellite data are given (Guo et al., 2004). The measured SO₂ concentration decreases with an e-folding time of 23±5 days (TOMS) and 25±5 days (TOVS). The simulated e-folding time of 33 days agrees however well to MLS satellite measurements (33 days) (Read et al., 1993) and previous TOMS data retrievals (35 days) of Bluth et al. (1992). The model does not include a full stratospheric chemistry. Therefore, possible influences of the volcanic eruption on OH and O₃ concentrations were not considered.

Figure 3 shows a slight overestimation of the simulated global SO₄²⁻ concentration maximum compared to HIRS measurements between 80° N and 80° S (Baran and Foot, 1994). The simulated concentration declines 200 days after the eruption when the measurements still remain on a higher level. One year after the eruption the simulated concentration is lower than the observed one. The onset of the declining concentration in the simulation coincides with the period of simulated maximum effective radius (r_{eff}) of the sulfate particle size distribution in the accumulation mode of 0.5 μm (Fig. 4). The effective radius increases earlier and the values are in the upper range of the measurements. This effect is even stronger at height levels between 12 and 16 km, indicating a faster accumulation of particles and stronger sedimentation. The decline of the simulated SO₄²⁻ concentration slows down about 500 days after the eruption, when r_{eff} becomes smaller than 0.4 μm.

Title Page

Abstract

Introduction

Conclusions

References

Tables

Figures

◀

▶

◀

▶

Back

Close

Full Screen / Esc

Printer-friendly Version

Interactive Discussion



Initial fate of fine ash

U. Niemeier et al.

[Title Page](#)[Abstract](#)[Introduction](#)[Conclusions](#)[References](#)[Tables](#)[Figures](#)[Back](#)[Close](#)[Full Screen / Esc](#)[Printer-friendly Version](#)[Interactive Discussion](#)

In Fig. 5, model results of the column mass are compared to lidar measurements taken in the northern mid latitude (Jäger et al., 1995). Measurements and model values increase with a similar slope. The maximum model concentration is reached one to two months earlier than in the measurements, indicating faster northward transport, and the period with maximum concentrations is shorter. Until about 450 days after the eruption, measurements and model data agree well. Thereafter the simulations show declining values while the measurements indicate again increasing values. This increase of the concentrations in the measurements showed in Fig. 5 is related to seasonal variations of the tropopause height (Timmreck et al., 1999) and must be regarded as an artefact of the analysis method.

The patterns of simulated Aerosol Optical Depth (AOD) (Fig. 6, top) are very similar to AVHRR and SAGE satellite measurements (Fig. 6, bottom). Both show maximum values along the equator and secondary maxima at 60° N. The model results also show a secondary maximum around 60° S with transport towards the pole after the southern polar vortex breaks down. In this area the satellite measurements also include a signal of the aerosols emitted by the August 1991 eruption of Cerro Hudson (45.9° S, 79.96° W), which is not included in the model simulation. It is noteworthy that the similar pattern in measurements and model results suggest a dominance of Pinatubo aerosol in the southern hemisphere and not of aerosols originating from Cerro Hudson. In the model results the tropical maximum is not persistent and the location of the maximum is half a year after the eruption north and not south of the equator as in the measurements. According to Trepte and Hitchman (1992) in the stratosphere exists an upper and a lower transport regime: below 50 hPa fast meridional poleward transport dominates, above 30 hPa one finds longer tropical residence times. Even though the aerosols stay above 50 hPa, the poleward transport in the model is overestimated. This is a model artefact and has also been shown in other model studies (Timmreck et al., 1999; Oman et al., 2006).

The simulated AOD is probably overestimated by 10 to 20%. Due to overestimated Sun photometer measurements, AVHRR measurements in 1991 should be corrected

by a factor of 0.84 (Russell et al., 1996). The AVHRR measurements show a maximum of 0.39 (uncorrected 0.47) and the simulated AOD maximum is 0.44. From the SAGE measurements even smaller values are reported, which were caused by an initial super-saturation of the instrument (Russell et al., 1996). One year after the eruption, SAGE data are more reliable and agree quite well with the simulated values. Our simulated spatio-temporal distribution of AOD agrees well with the observations, even though atmospheric dynamics were not forced to represent the actual dynamics of the years 1991–1993.

A comparison of the transport of ash and SO₂ clouds with satellite measurements (Guo et al., 2004) in the first days after the eruption shows a good representation of the transport in ECHAM5. Due to different injection heights, the ash cloud is advected slower to the west than the SO₂ cloud, similar to the observations. The simulated SO₂ cloud is advected slightly faster than observed. A second simulation with another eruption day and different wind conditions in the stratosphere (Pt1-5), agrees even better with the observations.

The grid resolution of the model is not sufficient to simulate the rotation of the umbrella cloud in the initial few hours, described in Holasek et al. (1996a) and Chakraborty et al. (2009). Baines et al. (2008) suggest a strong impact of this short-lasting rotation on the transport of the particles. Concluding from the good representation of transport in our results, this is not necessarily valid for the Mt. Pinatubo eruption.

5 Impact of fine ash on the radiation budget and its consequences for transport of sulfate

In this section the role of fine ash in the evolution of the volcanic cloud is investigated in more detail. This will be done for a tropical eruption (Pinatubo) and a Northern Hemispheric high latitude eruption (Katmai). For both we assume the strength of one and ten times the strength of the Pinatubo eruption. Because of the large particle radius, fine ash has a lifetime of only a few days (Fig. 1). We will therefore concentrate mainly

Title Page

Abstract

Introduction

Conclusions

References

Tables

Figures

◀

▶

◀

▶

Back

Close

Full Screen / Esc

Printer-friendly Version

Interactive Discussion



on the first days when the strongest impact can be assumed, but we also investigate longer lasting impacts of fine ash. The presented results base on an ensemble of five members and differences between simulations are significant. For an easier understanding of the plots, significant areas are only marked as grey areas in some plots.

5 Significance was calculated following the equations of a t-test.

5.1 Pinatubo simulation (Pt1_ens)

The vertically integrated aerosol optical depth of fine ash (AOD_A) is very high in the first days after the eruption (Fig. 7). Values above $AOD_A=7$ during the first day and 0.75 two days later are far above the values for sulfate. AOD_A decreases fast. After ten days the maximum AOD_A is 0.14, 0.03 after 20 days and 0.012 after 30 days, when the global fine ash concentration decreases to 0.6% of the emitted 100 Mt. Small amounts of fine ash stay even longer in the stratosphere and deposition of fine ash occurs globally still six months after the eruption.

15 The ash increased total AOD_A is causing an additional cooling at noon at the surface compared to a simulation with sulfate only. The air temperature 2 m above the surface (2 m-temperature) drops by one to two degrees over Indochina and India (Fig. 7, bottom) at noon local time (06:00 UTC) in the first three days after the eruption. Negligible influence of the ash particles on the 2-m temperature could be found in our simulations at night. There is not enough fine ash in the troposphere to cause nightly warming by

20 absorption of infrared radiation.

Figure 8 shows the daily averaged total radiative heating rates resulting from a simulation with fine ash (left) and without fine ash (right). They are calculated in the model via a twofold calculation of the radiation: once with all aerosols and once under clear sky conditions. Being initialised at a lower vertical level than SO_2 , two days after the eruption the heated ash cloud can be seen between 50 hPa and 100 hPa, with maximum heating rates slightly above 20 K/day. The sulfate layer on top of the ash is cooled, up to -10 K/day by outgoing longwave radiation, in both simulations. Values differ strongly between day and night. Especially in the first two days when the cloud

Title Page

Abstract

Introduction

Conclusions

References

Tables

Figures

◀

▶

◀

▶

Back

Close

Full Screen / Esc

Printer-friendly Version

Interactive Discussion



is very dense, cooling at night (-15 K/d) is very effective, overwhelming SW heating ($+5\text{ K/d}$) during the day in the daily mean. Also the positive heating rates below the sulfate layer are caused mainly by longwave radiation effects. The fine ash underneath increases the cooling by longwave radiation, similar as a strong cirrus cloud would do.

5 The strong cooling effect of the sulfate is turned towards a warming when dispersion decreases the sulfate concentration. With ongoing SO_2 oxidation the amount of sulfate increases and at day 10 the cloud is heated due to increasing effective radius of the particles, decreasing AOD, and sedimentation of ash. The effective radius of sulfate increases from $0.3\ \mu\text{m}$ in the first days after the eruption to $0.45\ \mu\text{m}$ after 5 days and $0.55\ \mu\text{m}$ after 10 days. When the fine ash is mainly sedimented after 10 days, only small differences in the cloud position can be seen, but still slightly less warming occurs underneath the sulfate cloud.

The presented simulations do not account for the UV and IR SO_2 absorption. Lary et al. (1994) calculated radiative heating rates of max 1.5 K/d for SO_2 , Gerstell et al. (1995) of 2 K/day . The conversion of SO_2 to sulfate takes place in the volcanic cloud and the two species are mixed and co-located. Therefore, we would expect a locally enhanced (over the sulfate) heating effect due to SO_2 . Anyhow, the radiative impact of ash is much stronger (daily heating of $>20\text{ K}$) dominating the radiative impact.

20 The influence of fine ash on the transport of the sulfur cloud is illustrated in Fig. 9. Here we give sulfur (S) to include the conversion of SO_2 to sulfate. The outer line represents a sulfur concentration of $2.5 \times 10^{-4}\text{ kg(S)/kg}$, the inner one varies to give an impression of the location of the maximum values. The differences between both simulations are small and within the 99% significance level. Six days after the eruption the cloud containing fine ash (blue line) shows a slightly increased transport towards the south and after 20 days (Fig. 9, bottom) the ash containing cloud is transported around the globe slightly quicker than without ash. Radiatively heated air expands, causing disturbances in the flow pattern. These disturbances differ for the cases with and without ash, resulting in varying dispersion and transport of the cloud.

Initial fate of fine ash

U. Niemeier et al.

[Title Page](#)[Abstract](#)[Introduction](#)[Conclusions](#)[References](#)[Tables](#)[Figures](#)[◀](#)[▶](#)[◀](#)[▶](#)[Back](#)[Close](#)[Full Screen / Esc](#)[Printer-friendly Version](#)[Interactive Discussion](#)

5.2 10 times Pinatubo (Pt10_ens)

We performed a sensitivity study applying ten times higher emissions to a Pinatubo eruption scenario (date, location, and emission rate of the eruption are those of Pinatubo) to see the influence of the emission strength on the impact of the fine ash. We obtain a 4 times higher total AOD_A for this scenario in the first days after the eruption (Fig. 10, top). The prescribed particle size distribution for fine ash emissions caused this linear response. The AOD_A rapidly decreases in the following days to values of 0.38 10 days after the eruption, 0.09 after 20 days, 0.035 after 30 days.

The maximum heating rates are increased compared to PT1 by a factor of two (Fig. 11), two days after the eruption and fine ash causes strong positive heating rates below the sulfate cloud. On the other hand, after five days the cooling and partly the heating of the sulfur cloud becomes more intense without fine ash. The additional heating of fine ash in the first two to three days after the eruption causes a stronger dispersion and an increased horizontal extension of the cloud. Therefore, the cloud without ash is more compact and stronger cooled and heated by radiative heating processes five and ten days after the eruption.

Compared to the non-ash case the 2-m-temperature is reduced by more than 3 K over Indochina two days after the eruption, and after three days also over India and Central Africa by 1 to 3 K cooler temperatures are simulated (Fig. 10, bottom)².

Figure 12 shows the sulfur burden for the 10 times Pinatubo simulations with and without fine ash. Both clouds are at the same location shortly after the eruption and differ stronger the following days. In radiatively heated areas the expanding air causes outflows (Fig. 13), in cooled areas we see an inflow. The ash containing cloud is stronger heated in the first days and dispersion of the cloud increases (Fig. 12, 3rd day). Six days after the eruption the ash containing cloud is transported about 3000 km farther to the west. The cloud without ash is more compact and stabilised by a small vortex in the area of the strongest heating (Fig. 13, bottom, 20° N, 50° E). The Coriolis

²The cooling is only seen over land as we used prescribed SSTs.

Title Page

Abstract

Introduction

Conclusions

References

Tables

Figures

◀

▶

◀

▶

Back

Close

Full Screen / Esc

Printer-friendly Version

Interactive Discussion



Initial fate of fine ashU. Niemeier et al.

[Title Page](#)[Abstract](#)[Introduction](#)[Conclusions](#)[References](#)[Tables](#)[Figures](#)[◀](#)[▶](#)[◀](#)[▶](#)[Back](#)[Close](#)[Full Screen / Esc](#)[Printer-friendly Version](#)[Interactive Discussion](#)

force causes a right turn of the expanding air. The vortex is stable for about two days. With ash, the heating in the further dispersed cloud is not sufficient to cause a rotation of expanding air even there are rotational movements in the vicinity of the volcanic cloud. The impact of the vortex diminishes with time and 20 days after the eruption the sulfur clouds show only small differences in their location. The northward shift in cloud position is caused by a slight vertical uplift of the cloud without ash into another wind regime. One month after the eruption transport of sulfate into the Southern Hemisphere is a factor 5 to 10 stronger with ash (between 30° S and 60° S). In these areas the sulfate concentrations are much smaller than in the tropics, where the differences remain below 50%.

We investigate the sensitivity of our results to changes in the meteorological situation by simulations with eruption dates five and ten days later. These simulations (Pt10-5) show similar results (not shown). Similar to the already described case, transport and wind speed increase in the first days when the cloud contains fine ash. Again the influence of ash vanishes with time and after 20 days the position of the cloud with and without ash is very similar. Different to the case Pt10_ens shown in Fig. 12, the Pt10-5 cases do not show the southward shift of the ash containing cloud. This is because Pt10-5 shows a smaller wind shear with height indicating the impact of weather on the initial dispersion of the stratospheric gases and aerosols.

5.3 Katmai simulation (Kat1_ens)

Comparing wind patterns of several years taken from a climatological MAECHAM5 simulation, the typical meteorological situation in southern Alaska, the area of the Mt. Katmai volcano, is determined by a strong vertical wind shear in the stratosphere in June. South-westerly to north-westerly winds are prevailing in the lower stratosphere, turning to south-easterly to northeasterly winds above 50 hPa and easterly above 25 hPa. This general pattern can be disturbed by cyclones, causing variations between more northerly and southerly wind directions influencing the prevailing easterly or westerly flow. The mean wind speed is below 10 m/s, much lower than in the tropics. We present

simulations with two different eruption dates to consider the influence of specific meteorological situations.

Figure 14 shows the aerosol optical depth of ash. AOD_A values maintain high during the first week which is related to low dispersion of the cloud and low stratospheric wind speeds. Figure 14 indicates also the transport of fine volcanic ash along the northern coast of Alaska towards Canada. The ash is emitted at 50 hPa and sedimented quickly to lower levels. It is therefore affected by the south-westerly winds. In contrast, Fig. 15 (top) shows that the SO_2 cloud, being injected into the level above 30 hPa, is transported towards Siberia. The wind-shear clearly separates fine ash and sulfur due to changing transport directions in different levels.

Values of daily heating rates in simulation Kat1_ens (Fig. 16) are in a similar range as PT1. The westward drifting ash cloud can well be seen in the first column, middle and lower plot, east of $150^\circ W$. As ash and sulfate are separated, the heating rates for the sulfate cloud are quite similar in both simulations. Variations are mainly caused by the different transport direction of the sulfate clouds. In order to capture the main impact of the heating rates, the cross sections in Fig. 16 were taken at increasing latitudes.

In general, the volcanic cloud stays close to the origin. This is caused by low wind speeds, as well as by the development of a rotational movement inside of the volcanic cloud starting about two days after the eruption (Fig. 17). A difference to the Pt10_ens case is a weaker stratospheric main flow and a stronger Coriolis force. Thus, the impact of the heated ash cloud causes an early development of a vortex in the ash containing level. The rotating cloud is slowly advected with the main wind. Due to the lower dispersion the cloud is very dense and outgoing longwave radiation is dominating the radiative processes even longer than in Pt1_ens.

During the first 5 days differences between the simulation with and without ash are small. After 5 days the ash cloud is clearly separated from the sulfate cloud and is transported to the east. The sulfate cloud is transported farther northeastward in the simulation with ash and is dispersed over a larger area. Therefore sulfate concentration and radiative heating are smaller than without ash. The 2 m-temperature is two degrees

Initial fate of fine ash

U. Niemeier et al.

Title Page

Abstract

Introduction

Conclusions

References

Tables

Figures

◀

▶

◀

▶

Back

Close

Full Screen / Esc

Printer-friendly Version

Interactive Discussion



lower than in the simulation without ash in a small area close to the volcano.

The radiative heating and cooling of the volcanic cloud are causing vertical movements inside the cloud. Figure 18 shows the vertical velocity developing over the first eleven days. Solar heating during the day causes a rising of the cloud, partly compensating ash sedimentation. During the night downward motion dominates and ash sedimentation is stronger. In the simulation without ash the effects of these vertical movements are much smaller.

To investigate a different meteorological situation, a simulation with an eruption five days later was performed (Kat1-5). Figure 15 (bottom) shows the calculated sulfate concentration for this second simulation for the cases with and without ash. The results differ only slightly from the previous case. The additional heating of the ash is causing a somewhat stronger influence of the volcanic cloud on the local wind field. Parts of the sulfate cloud, at about 40 hPa to 60 hPa, are advected to the south east, which is not the case in the simulation excluding the ash.

5.4 10 times Katmai (Kat10_ens)

Increasing the emissions at the Katmai volcano to 10× Pinatubo increases the radiative heating of the cloud causing an intensified rotation of the cloud. Figure 19 shows the maximum of the sulfur clouds with and without fine ash two weeks after the eruption. The cloud containing ash is advected about 1500 km to the north in 14 days, which is a very short transport distance compared to the previous results Pt1_ens, Pt10_ens and Kat1_ens. The increased amount of volcanic aerosol that can be heated by long and shortwave absorption, stabilises the rotation of the cloud and keeps it much longer active, inhibiting the exchange with the surrounding flow. Seven days after the eruption the radiative forcing in the centre of the cloud is still large (15 K/day) and the wind velocity in the rotating cloud is almost twice as high as without ash. The extension of the vortex containing ash is larger in horizontal and vertical direction. Five days later, with ash the wind speed in the vortex is still similar. The non ash containing vortex broke down already. Central parts of the cloud are radiatively cooled and a small

Initial fate of fine ash

U. Niemeier et al.

Title Page

Abstract

Introduction

Conclusions

References

Tables

Figures



Back

Close

Full Screen / Esc

Printer-friendly Version

Interactive Discussion



cyclonic vortex develops.

The rotating volcanic cloud changes also the transport and lifetime of the ash. Figure 20 shows the AOD_A of ash 1, 10 and 16 days after the eruption with the maximum concentration about 1000 to 2000 km north of the eruption location. Farther transported are only parts of the ash which have been sedimented to lower vertical heights. The cloud remains more compact compared to the Pinatubo case and therefore the AOD_A of the ash is higher for the first twenty days, causing a stronger heating and increased impact of the ash.

5.5 Impact of fine ash on sulfate evolution

Figure 21 shows a comparison of total global sulfate concentration of simulation Pt1 and Kat1, both with and without fine ash. The longterm impact of the fine ash is small. The sulfate concentrations differ by less than one percent whether ash is included or not. The sulfate particle radius is very similar in Pt1 between the ash and non-ash case. In Kat1 the effective radius differs between 0.05 and 0.1 μm and is smaller in the simulation with ash in the first three months. The particle radius depends on the sulfur concentration which at the higher northern latitudes differs stronger locally between an ash and non-ash simulation. However we did not take into account any heterogeneous nucleation of sulfuric acid and water on the fine ash particles. Similar to dust, coated fine ash particles might act as sink via condensation and coagulation and therefore modify the aerosol size distribution (Korhonen et al., 2003).

The lifetime of sulfate is shorter in the eruption in Alaska compared to the sulfate lifetime after the eruption of Mt. Pinatubo. Here the Brewer-Dobson-circulation with downward transport at high Northern latitudes plays a role. Also the principally larger effective radius, about 0.15 μm as a zonal mean value, increases the sedimentation. The sulfate cloud is not advected over both hemispheres, causing higher concentrations than after a tropical eruption. Also the conditions for the aerosol microphysics differ. The longer polar day and therefore longer active OH chemistry does not have an effect on the lifetime of SO_2 .

Title Page

Abstract

Introduction

Conclusions

References

Tables

Figures

◀

▶

◀

▶

Back

Close

Full Screen / Esc

Printer-friendly Version

Interactive Discussion



6 Conclusions

The simulated evolution of the sulfur and fine ash aerosol cloud after the eruption of Mt. Pinatubo was compared to satellite and lidar measurements. Overall, measurements and simulation results agree very well for the aerosol optical depth and effective radius of the particle, even though differences can be seen in some details. The particle radius strongly determines the sedimentation and therefore the lifetime of sulfate aerosol in the stratosphere. The particle radius is in the upper range of the measurements, causing a return to pre-eruption values about 6 months earlier than observed. The AOD of sulfate shows compared to measurements qualitatively and quantitatively very good results.

The influence of fine volcanic ash on the climatic impact of a volcanic eruption is small. The lifetime of ash is too short to have an influence itself and changes in the global sulfate concentration due to the presence of fine ash are below one percent. However, in the first two weeks after the eruption, fine ash is important as the ash changes the wind pattern in the vicinity of the cloud. This impact depends on the strength of the undisturbed stratospheric wind. It is smaller in the tropics where the wind velocity is higher than at higher latitudes.

The impact of the ash is well detectable in the first two weeks after the eruption and is stronger in the simulation of a Katmai eruption compared to the eruption of the Mt. Pinatubo in the tropics. The longterm impact of the ash via sulfate particle radii and concentration, caused by different SO_2 concentration in the early phase after the eruption, is negligible.

Volcanic fine ash with a size smaller than $15 \mu\text{m}$ has a lifetime of a few days to weeks in the stratosphere, causing the main impact during the first days after the eruption. Fine ash is normally placed underneath the SO_2 cloud and an additional radiative heating below the sulfate cloud is found in this period. This heating causes strong disturbances in flow pattern, changing wind direction and increasing wind speed. The impact of this additional motion strongly depends on the location, time and strength of

Initial fate of fine ash

U. Niemeier et al.

Title Page

Abstract

Introduction

Conclusions

References

Tables

Figures



Back

Close

Full Screen / Esc

Printer-friendly Version

Interactive Discussion



the eruption. At the surface the 2 m-temperature is further decreased by about 2 K due to the additional ash in the first three days.

In the tropics, the local impact of the additional radiative heating of the fine ash is too weak to interfere with the prevailing easterlies in a QBO east phase and monsoon winds. In the 1 × Pinatubo case we see only small impact of fine ash on local winds and on the transport of the volcanic aerosol cloud. In the 10 × stronger eruption case, the ash caused a stronger dispersion and increased advection. Without ash the volcanic cloud is more compact. Five to six days after the eruption a small vortex is further stabilising the cloud and reducing advection. Thereby increasing difference to the ash case.

At 60° N, at the position of Mt. Katmai, the situation is different, because the local flow is weaker and the Coriolis-Force is stronger. The latter causes a clockwise rotation of the aerosol cloud due to expanding heated air. Due to this rotation the volcanic cloud is less dependent on the surrounding flow, stays closer to the origin and horizontal dispersion is reduced. The ash causes an vertical expansion of the heated area also below the sulfate cloud, which increases the vertical extension of the rotating mass. Due to increased uplifting of the sulfate and changing wind direction with height, together with increased wind speed, the transport direction of the sulfate cloud changes due to the presence of fine ash.

The described interaction between regional wind field and the volcanic aerosol occurs via radiative heating. The radiative heating of the aerosol has a strong impact on the behaviour of the cloud, e.g. by inducing vertical motion and horizontal expansion. Radiative heating induced rotation of the cloud diminishes advection. Without radiative heating processes, the regional wind fields are not influenced by the volcanic cloud. In the case of large eruptions the model could not correct simulate the transport and sedimentation of ash nor the long-range transport of the sulfate cloud (Timmreck and Graf, 2006). Therefore the coupling of the aerosol with solar and terrestrial radiation is necessary. The simulation of ash and sulfate is important when studying the short term impacts of a large volcanic eruption reaching the stratosphere.

Initial fate of fine ash

U. Niemeier et al.

Title Page

Abstract

Introduction

Conclusions

References

Tables

Figures



Back

Close

Full Screen / Esc

Printer-friendly Version

Interactive Discussion



Acknowledgements. This work contributed to the Super Volcano project at the Max-Planck Institute for Meteorology. U. Niemeier is partially supported by SCOUT-O3 and CLISAP. C. Timmreck acknowledges founding from the German Science Foundation DFG grant TI 344/1-1. We further thank R. Hommel, J. Kazil, H. Kokkola and H. Vehkamäki for their help to modify HAM.

The service charges for this open access publication have been covered by the Max Planck Society.

References

- Ansmann, A., Mattis, I., Wandinger, U., Wagner, F., Reichardt, J., and Deshler, T.: Evolution of the Pinatubo Aerosol: Raman Lidar Observations of Particle Optical Depth, Effective radius, Mass, and Surface Area over Central Europe at 53.4 N, *JAS*, 54, 2630–2641, 1997. 17560
- Baines, P. G., Jones, M. T., and Sparks, R. S. J.: The variation of large-magnitude volcanic ash cloud formation with source latitude, *J. Geophys. Res.*, 113, D21204, doi:10.1029/2007JD009568, 2008. 17541
- Baran, A. J. and Foot, J. S.: New application of the operational sounder HIRS in determining a climatology of sulphuric acid aerosol from the Pinatubo eruption, *J. Geophys. Res.*, 99, 673–679, 1994. 17539, 17559
- Bluth, G. J. S., Doiron, S. D., Schnetzler, C. C., Krueger, A. J., and Walte, L. S.: Global tracking of the SO₂ clouds from the June, 1991 Mount Pinatubo eruptions, *Geophys. Res. Lett.*, 19, 151–154, 1992. 17539
- Chakraborty, P., Gioia, G., and Kieffer, S. W.: Volcanic mesocyclones, *Nature*, 458, 497–500, doi:10.1038/nature07866, 2009. 17541
- Duggen, S., Croot, P., Schacht, U., and Hoffmann, L.: Subduction zone volcanic ash can fertilize the surface ocean and stimulate phytoplankton growth: Evidence from biogeochemical experiments and satellite data, *Geophys. Res. Lett.*, 34, doi:10.1029/2006GL027522, 2007. 17533
- Feichter, J., Kjellstrom, E., Rohde, H., Dentener, F., Lelieveld, J., and Roelofs, G. J.: Simulation of the tropospheric sulfur cycle in a global climate model, *Atmos. Environ.*, 30, 1693–1707, 1996. 17536

Initial fate of fine ash

U. Niemeier et al.

Title Page

Abstract

Introduction

Conclusions

References

Tables

Figures

◀

▶

◀

▶

Back

Close

Full Screen / Esc

Printer-friendly Version

Interactive Discussion



Initial fate of fine ash

U. Niemeier et al.

[Title Page](#)[Abstract](#)[Introduction](#)[Conclusions](#)[References](#)[Tables](#)[Figures](#)[◀](#)[▶](#)[◀](#)[▶](#)[Back](#)[Close](#)[Full Screen / Esc](#)[Printer-friendly Version](#)[Interactive Discussion](#)

- Fero, J., Carey, S. N., and Merrill, J. T.: Simulation of the 1980 eruption of Mount St. Helens using the ash-tracking model PUFF, *J. Jvolgeores*, 175, 355–366, doi:10.1016/j.jvolgeores.2008.03.029, 2008. 17534
- Folch, A., Jorba, O., and Viramonte, J.: Volcanic ash forecast - application to the May 2008 Chaitén eruption, *Nat. Hazards Earth Syst. Sci.*, 8, 927–940, 2008, <http://www.nat-hazards-earth-syst-sci.net/8/927/2008/>. 17534
- Gerstell, M., Crisp, J., and Crisp, D.: Radiative Forcing of the Stratosphere by SO₂ Gas, Silicate Ash, and H₂SO₄ Aerosols Shortly after the 1982 Eruptions of El Chichón, *J. Climate*, 8, 1060–1070, doi:10.1175/1520-0442(1995)008<1060RFOTSB>2.0.CO;2, 1995. 17543
- Giorgetta, M. A., Manzini, E., Roeckner, E., Esch, M., and Bengtsson, L.: Climatology and forcing of the quasi-biennial oscillation in the MAECHAM5 model, *J. Climate*, 19, 3882–3901, 2006. 17535
- Guo, S., Rose, W. I., Bluth, G. J. S., and Watson, I. M.: Particles in the great Pinatubo volcanic cloud of June 1991: The role of ice, *Geochem. Geophys. Geosy.*, 5, Q05003, doi:10.1029/2003GC000655, 2004. 17533, 17537, 17538, 17539, 17541, 17557, 17559
- Herzog, M., Graf, H. F., Textor, C., and Oberhuber, J. M.: The effect of phase changes of water on the development of volcanic plumes, *J. Volcanol. Geoth. Res.*, 87, 55–74, 1998. 17534
- Holasek, R. E., Self, S., and Woods, A. W.: Satellite observations and interpretation of the 1991 Mount Pinatubo eruption plumes, *J. Geophys. Res.*, 101(B12), 635–655, 1996a. 17541
- Holasek, R. E., Woods, A., and Self, S.: Experiments on gas-ash separation processes in volcanic umbrella clouds, *J. Volcanol. Geotherm. Res.*, 70, 169–181, 1996b. 17537
- Jäger, H., Uchino, O., Nagai, T., Fujimoto, T., Freudenthaler, V., and Homburg, F.: Ground-based remote sensing of the decay of the Pinatubo eruption cloud at three Northern Hemisphere sites, *Geophys. Res. Lett.*, 22, 607–610, 1995. 17540, 17561
- Jöckel, P., Sander, R., Kerkweg, A., Tost, H., and Lelieveld, J.: Technical Note: The Modular Earth Submodel System (MESSy) – a new approach towards Earth System Modeling, *Atmos. Chem. Phys.*, 5, 433–444, 2005, <http://www.atmos-chem-phys.net/5/433/2005/>. 17536
- Jones, M., Sparks, R. S. J., and Valdes, P. J.: The climatic impact of supervolcanic ash blankets, *Clim. Dynam.*, 29, 553–564, doi:10.1007/s00382-007-0248-7, 2007. 17533
- Kirchner, I., Stenchikov, G. L., Graf, H.-F., Robock, A., and Antuña, J. C.: Climate model simulation of winter warming and summer cooling following the 1991 Mount Pinatubo volcanic eruption, *J. Geophys. Res.*, 104, 19039–19056, 1999. 17532

Initial fate of fine ashU. Niemeier et al.

[Title Page](#)[Abstract](#)[Introduction](#)[Conclusions](#)[References](#)[Tables](#)[Figures](#)[◀](#)[▶](#)[◀](#)[▶](#)[Back](#)[Close](#)[Full Screen / Esc](#)[Printer-friendly Version](#)[Interactive Discussion](#)

- Kokkola, H., Hommel, R., Kazil, J., Niemeier, U., Partanen, A.-I., Feichter, J., and Timmreck, C.: Aerosol microphysics modules in the framework of the ECHAM5 climate model - intercomparison under stratospheric conditions, *Geosci. Model Dev. Discuss.*, 2, 209–246, 2009. 17536
- 5 Korhonen, H., Napari, I., Timmreck, C., Vehkamäki, H., Pirjola, L., Lehtinen, K., Lauri, A., and Kulmala, M.: Impact of sulphate coating mineral dust on new particle formation: A model study of heterogeneous nucleation, *J. Geophys. Res.*, D20, 8791, doi:10.1029/2002JD003167, 2003. 17548
- 10 Krueger, A. J., Walter, L. S., Bhartia, P. K., Schnetzler, C. C., Krotkov, N. A., Sprod, I., and Bluth, G. J. S.: Volcanic sulfur dioxide measurements from the total ozone mapping spectrometer instrument, *J. Geophys. Res.*, 100, 14057–14076, 1995. 17536
- Lary, B., Balluch, M., and Bekki, S.: Solar heating after volcanic eruption: The importance of SO₂ absorption, *Q. J. Roy. Meteor. Soc.*, 120, 1683–1688, 1994. 17543
- 15 Lin, S. J. and Rood, R. B.: Multidimensional flux form semi-Lagrangian transport, *Mon. Weather Rev.*, 124, 2046–2068, 1996. 17535
- Oman, L., Robock, A., Stenchikov, G. L., Thordarson, T., Koch, D., Shindell, D. T., and Gao, C.: Modeling the distribution of the volcanic aerosol cloud from the 1783–1784 Laki eruption, *J. Geophys. Res.*, 111, D12209, doi:10.1029/2005JD006899, 2006. 17532, 17540
- 20 Pollack, J. R., Toon, O. B., and Khare, B.: Optical Properties of Some Terrestrial Rocks and Glasses, *Icarus*, 19, 372–389, 1973. 17535
- Prata, A. J. and Kerkmann, J.: Simultaneous retrieval of volcanic ash and SO₂ using MSG-SEVIRI measurements, *Geophys. Res. Lett.*, 34, L05813, doi:10.1029/2006GL028691, 2007. 17533
- 25 Read, W. G., Froidevaux, L., and Waters, J. W.: Microwave limb sounder measurements of stratospheric SO₂ from the Mt. Pinatubo volcano, *Geophys. Res. Lett.*, 20, 1299–1302, 1993. 17536, 17539
- Roeckner, E., Baeuml, G., Bonaventura, L., Brokopf, R., Esch, M., Giorgetta, M., Hagemann, S., Kirchner, I., Kornblueh, L., Manzini, E., Rhodin, A., Schlese, U., Schulzweida, U., and Tompkins, A.: The atmospheric general circulation model ECHAM5 – Part I, *MPI Report No. 349*, p. 127, 2003. 17535
- 30 Russell, P. B., Livingston, J. M., Pueschel, R. F., Pollack, J. B., Brooks, S., Hamill, P., Hughes, J., Thomason, L., Stowe, L., Deshler, T., and Dutton, E.: Global to microscale evolution of the Pinatubo volcanic aerosol, derived from diverse measurements and analyses, *J. Geophys.*

Initial fate of fine ash

U. Niemeier et al.

[Title Page](#)[Abstract](#)[Introduction](#)[Conclusions](#)[References](#)[Tables](#)[Figures](#)[◀](#)[▶](#)[◀](#)[▶](#)[Back](#)[Close](#)[Full Screen / Esc](#)[Printer-friendly Version](#)[Interactive Discussion](#)

Res., 101, 18745–18763, 1996. 17541

Schneider, D. J., Rose, W. I., Coke, L. R., Bluth, G. J. S., Sprod, I. E., and Krueger, A. J.: Early evolution of a stratospheric volcanic eruption cloud as observed with TOMS and AVHRR, *J. Geophys. Res.*, 104(D4), 4037–4050, doi:10.1029/1998JD200073, 1999. 17537

5 Searcy, C., Dean, K., and Stringer, W.: PUFF: A high-resolution volcanic ash tracking model, *J. Volcanol. Geoth. Res.*, 80, 1–16, 1998. 17534

Self, S.: The effect and consequences of very large explosive volcanic eruptions, *Philos. T. Roy. Soc. A*, 364, 2073–2097, doi:10.1098/rsta.2006.1814, 2006. 17533

10 Stenchikov, G. L., Kirchner, I., Robock, A., Graf, H.-F., Antuña, J. C., Grainger, R. G., Lambert, A., and Thomason, L.: Radiative forcing from the 1991 Mount Pinatubo volcanic eruption, *J. Geophys. Res.*, 103, 13837–13858, 1998. 17532

Stier, P., Feichter, J., Kinne, S., Kloster, S., Vignati, E., Wilson, J., Ganzeveld, L., Tegen, I., Werner, M., Balkanski, Y., Schulz, M., Boucher, O., Minikin, A., and Petzold, A.: The aerosol-climate model ECHAM5-HAM, *Atmos. Chem. Phys.*, 5, 1125–1156, 2005, <http://www.atmos-chem-phys.net/5/1125/2005/>. 17535, 17536

15 Suzuki, Y. J. and Koyaguchi, T.: A three-dimensional numerical simulation of spreading umbrella clouds, *J. Geophys. Res.*, 114(B03), 209, doi:10.1029/2007JB005369, 2009. 17534

Textor, C., Graf, H. F., Herzog, M., Oberhuber, J. M., Rose, W. I., and Ernst, G. G. J.: Volcanic particle aggregation in explosive eruption columns, Part I: Parameterization of the microphysics of hydrometeors and ash, *J. Volcanol. Geoth. Res.*, 150, 359–377, doi:10.1016/j.jvolgeores.2005.09.007, 2006. 17534

20 Thomas, M. A., Giorgetta, M. A., Timmreck, C., Graf, H.-F., and Stenchikov, G.: Simulation of the climate impact of Mt. Pinatubo eruption using ECHAM5 - Part 2: Sensitivity to the phase of the QBO and ENSO, *Atmos. Chem. Phys.*, 9, 3001–3009, 2009, <http://www.atmos-chem-phys.net/9/3001/2009/>. 17532

25 Timmreck, C. and Graf, H.-F.: The initial dispersal and radiative forcing of a Northern Hemisphere mid-latitude super volcano: a model study, *Atmos. Chem. Phys.*, 6, 35–49, 2006, <http://www.atmos-chem-phys.net/6/35/2006/>. 17550

Timmreck, C., Graf, H.-F., and Kirchner, I.: A one and half year interactive MA/ECHAM4 simulation of Mount Pinatubo Aerosol, *J. Geophys. Res.*, 104, 9337–9360, doi:10.1029/1999JD900088, 1999. 17532, 17540

30 Timmreck, C., Graf, H.-F., and Steil, B.: Aerosol chemistry interactions after the Mt. Pinatubo eruption, in *Volcanism and the Earth's Atmosphere*, AGU Monograph 139, pp. 214–225,

2003. 17532, 17536

Trepte, C. R. and Hitchman, M. H.: Tropical stratospheric circulation deduced from satellite aerosol data, *Nature*, 355, 626–628, 1992. 17540

5 Tupper, A., Carn, S., Davey, J., Kamada, Y., Potts, R., Prata, F., and Tokuno, M.: An evaluation of volcanic cloud detection techniques during recent significant eruptions in the western Ring of Fire, *Remote Sens. Environ.*, 91, 27–46, doi:10.1016/j.rse.2004.02.004, 2004. 17534

Vignati, E., Wilson, J., and Stier, P.: M7: An efficient size resolved aerosol micro-physics module for large-scale aerosol transport models, *J. Geophys. Res.*, 109, D22202, doi:10.1029/2003JD004485, 2004. 17536

10 Wen, S. and Rose, W. I.: Retrieval of sizes and total masses of particles in volcanic clouds using AVHRR bands 4 and 5, *J. Geophys. Res.*, 99, 5421–5431, 1994. 17537

Wiesner, M., Wetzel, A., Catane, S. G., Listanco, E., and Mirabueno, H. T.: Grain size, areal thickness distribution and controls on sedimentation of the 1991 Mt. Pinatubo tephra layer in the South China Sea, *B. Volcanol.*, 66, 226–242, 2004. 17533, 17538, 17558

Initial fate of fine ash

U. Niemeier et al.

Title Page

Abstract

Introduction

Conclusions

References

Tables

Figures



Back

Close

Full Screen / Esc

Printer-friendly Version

Interactive Discussion



Initial fate of fine ash

U. Niemeier et al.

Table 1. Simulations performed for the two different volcanic eruption sites. Pt1_ens, Kat1_ens, Pt10_ens and Kat10_ens contain each an ensemble of five simulations. For both sites total emissions comparable to the Mt. Pinatubo eruptions are assumed: 1×: emissions of 17 Mt SO₂ and 100 Mt fine ash in 3 h; 10×: emissions of 1700 Mt SO₂ and 10 000 Mt fine ash in 30 h.

Eruption date	June 1st		June 5th and 10th	
Eruption strength	1×	10×	1×	10×
Pinatubo	Pt1_ens	Pt10_ens	Pt1-5	Pt10-5
Katmai	Kat1_ens	Kat10_ens	Kat1-5	

Title Page

Abstract

Introduction

Conclusions

References

Tables

Figures

◀

▶

◀

▶

Back

Close

Full Screen / Esc

Printer-friendly Version

Interactive Discussion



Initial fate of fine ash

U. Niemeier et al.

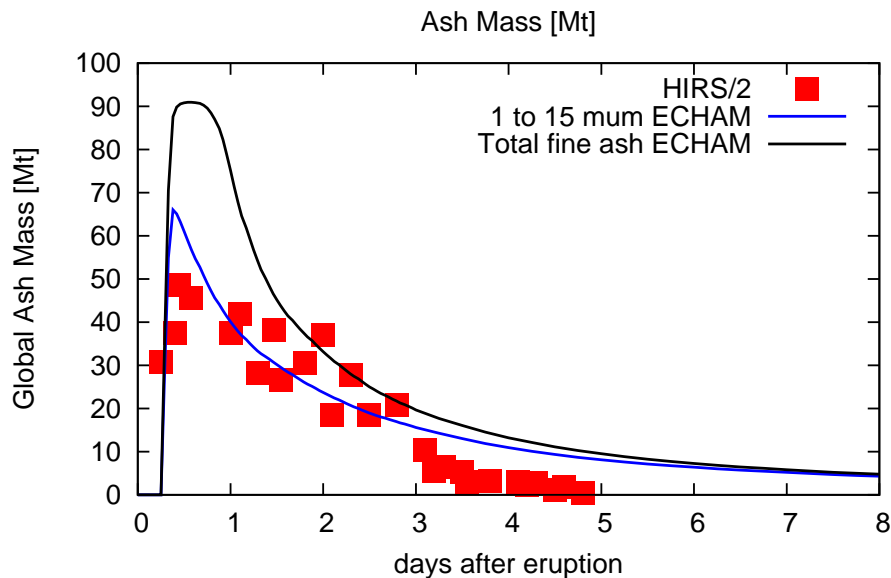
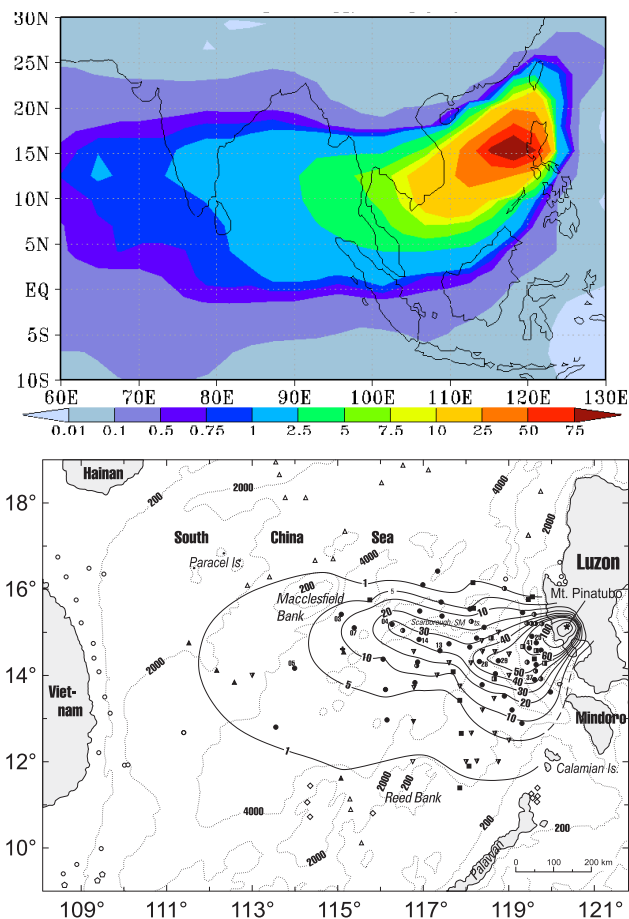


Fig. 1. Evolution of the global mass of fine ash in the first days after the Mt. Pinatubo eruption. The red squares show results of satellite measurements in the size range of $1\ \mu\text{m}$ to $15\ \mu\text{m}$ (Guo et al., 2004), the curves give model results of the total fine ash amount (black) and the amount of fine ash in the $1\ \mu\text{m}$ to $15\ \mu\text{m}$ size interval.

[Title Page](#)[Abstract](#)[Introduction](#)[Conclusions](#)[References](#)[Tables](#)[Figures](#)[◀](#)[▶](#)[◀](#)[▶](#)[Back](#)[Close](#)[Full Screen / Esc](#)[Printer-friendly Version](#)[Interactive Discussion](#)

Initial fate of fine ash

U. Niemeier et al.



Initial fate of fine ash

U. Niemeier et al.

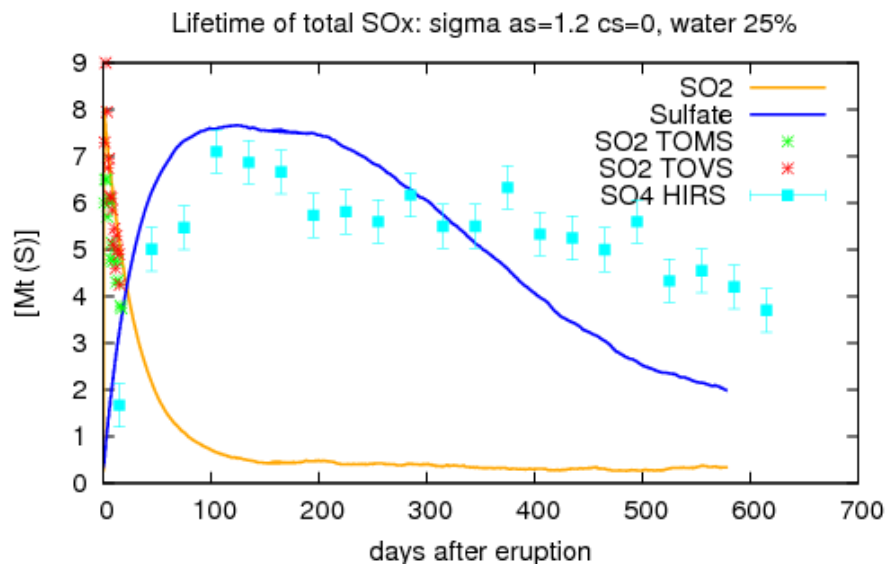


Fig. 3. Global mass of SO₂ and sulfate in the MAECHAM5-HAM simulations (lines) and satellite measurements (HIRS) (Baran and Foot, 1994), TOMS and TOVS (Guo et al., 2004) after the Pinatubo eruption.

[Title Page](#)[Abstract](#)[Introduction](#)[Conclusions](#)[References](#)[Tables](#)[Figures](#)[◀](#)[▶](#)[◀](#)[▶](#)[Back](#)[Close](#)[Full Screen / Esc](#)[Printer-friendly Version](#)[Interactive Discussion](#)

Initial fate of fine ash

U. Niemeier et al.

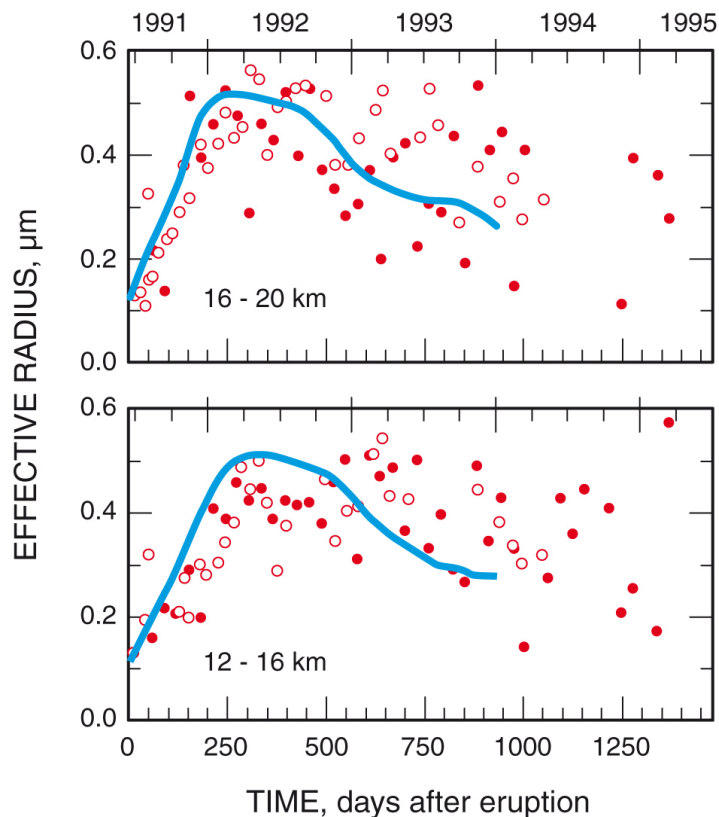


Fig. 4. Effective radius at Northern Hemisphere mid latitudes after the Pinatubo eruption. The circles represent lidar measurements at Laramie 41° N (open circle) and Geesthacht 53.4° N (closed circle) (Ansmann et al., 1997) and the blue line zonal mean model results at 53° N.

[Title Page](#)[Abstract](#)[Introduction](#)[Conclusions](#)[References](#)[Tables](#)[Figures](#)[◀](#)[▶](#)[◀](#)[▶](#)[Back](#)[Close](#)[Full Screen / Esc](#)[Printer-friendly Version](#)[Interactive Discussion](#)

Initial fate of fine ash

U. Niemeier et al.

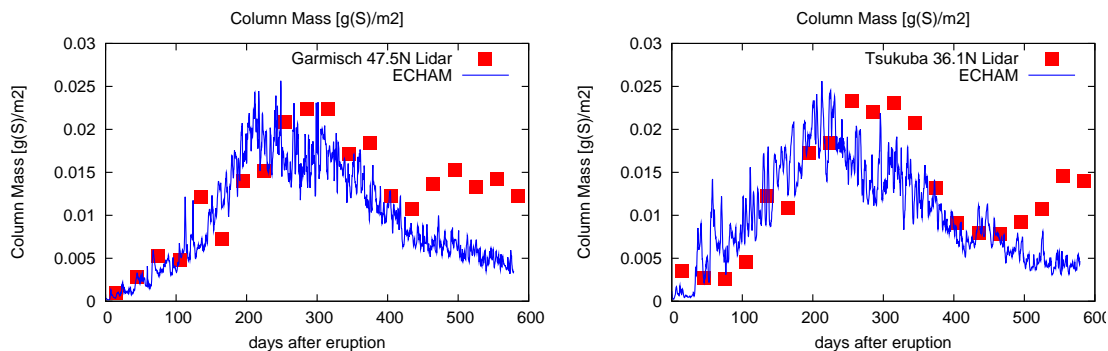


Fig. 5. Monthly mean column mass of sulfate [g(S)/m^2] after the Mt. Pinatubo eruption. Lidar measurements at Garmisch (47.5°N) and Tsukuba (36.1°N) (Jäger et al., 1995) are indicated as red squares and simulated values for the corresponding model grid as blue lines.

[Title Page](#)[Abstract](#)[Introduction](#)[Conclusions](#)[References](#)[Tables](#)[Figures](#)[◀](#)[▶](#)[◀](#)[▶](#)[Back](#)[Close](#)[Full Screen / Esc](#)[Printer-friendly Version](#)[Interactive Discussion](#)

Initial fate of fine ash

U. Niemeier et al.

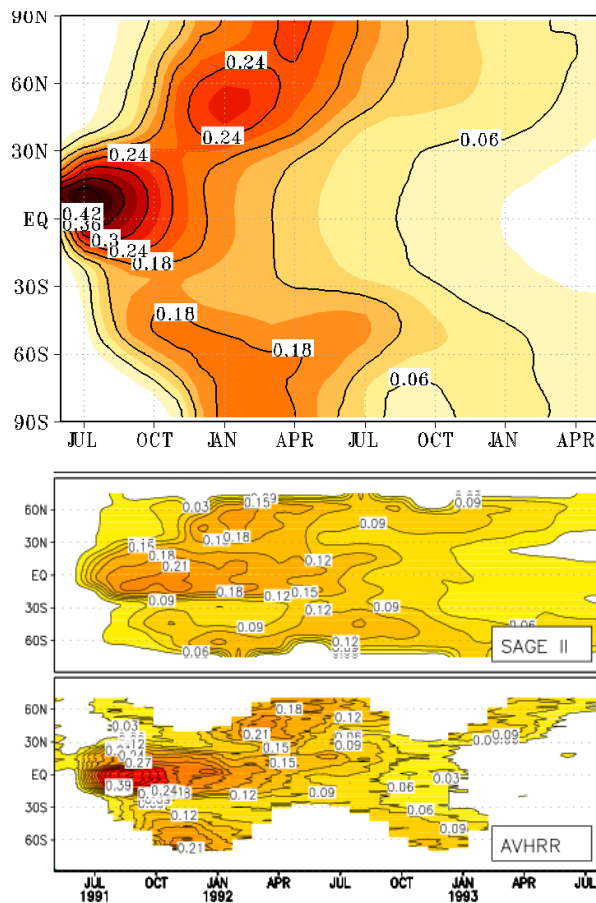


Fig. 6. Aerosol optical depth at $0.55 \mu\text{m}$, model results (top), SAGE data (middle), AVHRR data (bottom).

[Title Page](#)[Abstract](#)[Introduction](#)[Conclusions](#)[References](#)[Tables](#)[Figures](#)[◀](#)[▶](#)[◀](#)[▶](#)[Back](#)[Close](#)[Full Screen / Esc](#)[Printer-friendly Version](#)[Interactive Discussion](#)

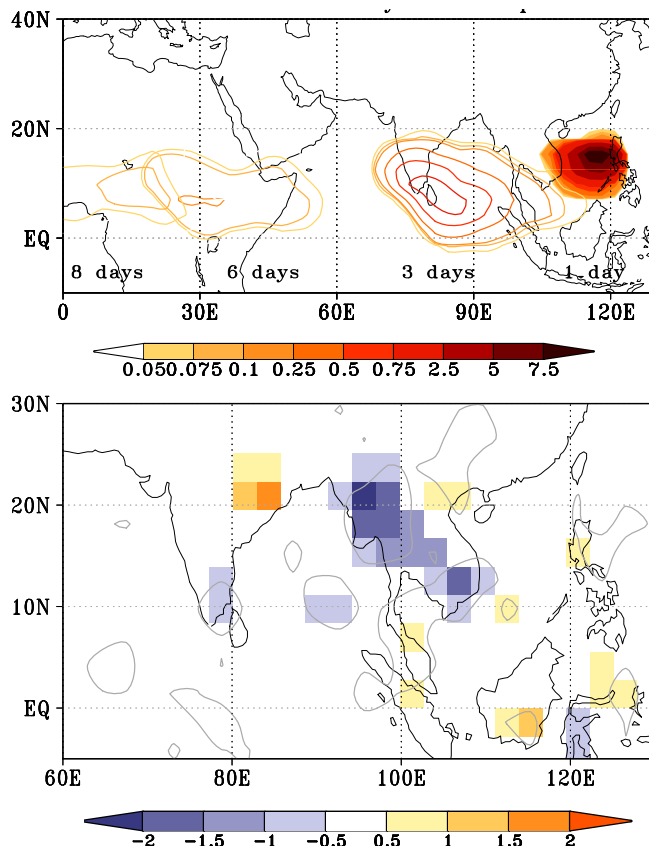


Fig. 7. Development of the aerosol optical depth of fine ash over the first week after the Mt. Pinatubo eruption (top) and differences in the 2-m-temperature [K] comparing the simulation with and without ash (bottom) at the 3rd day after the eruption at noon local time (Case Pt1_ens). The grey line denotes the 99% significance level.

[Title Page](#)[Abstract](#)[Introduction](#)[Conclusions](#)[References](#)[Tables](#)[Figures](#)[◀](#)[▶](#)[◀](#)[▶](#)[Back](#)[Close](#)[Full Screen / Esc](#)[Printer-friendly Version](#)[Interactive Discussion](#)

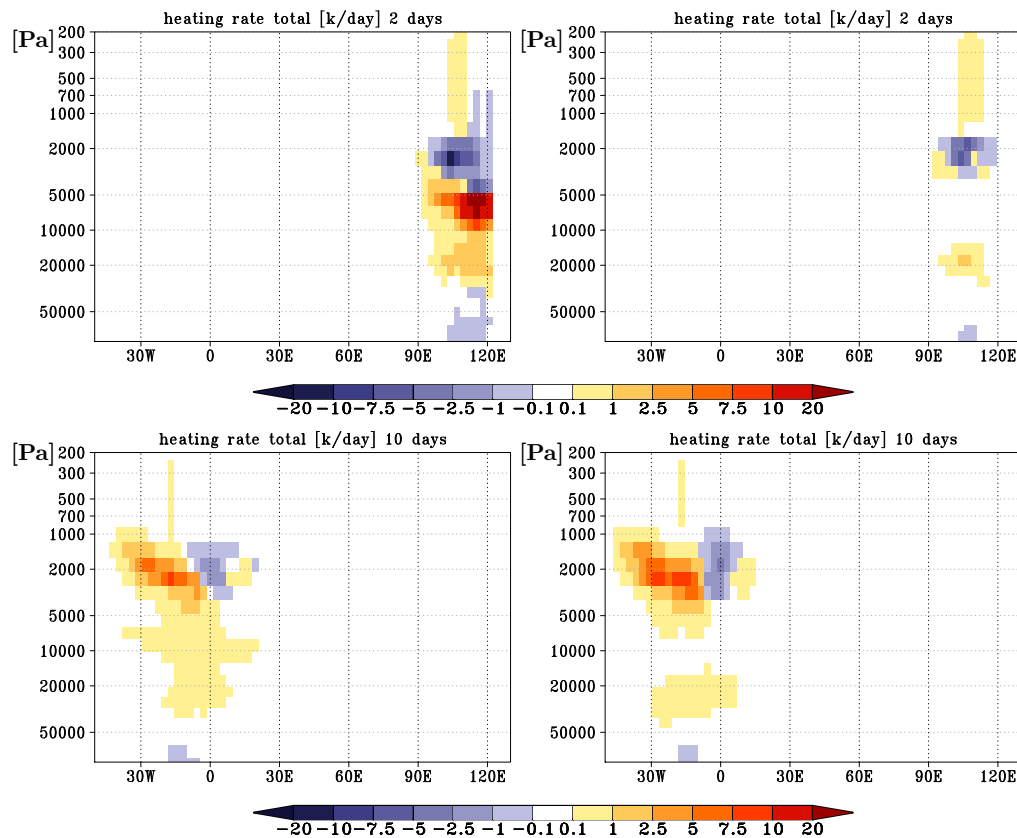


Fig. 8. Total radiative heating rates [K/day] as a daily mean two days (top) and ten days (bottom) after the Mt. Pinatubo eruption (Pt1_ens) in a simulation including fine ash (left) and without fine ash (right). Given is a vertical cross section along 15° N.

[Title Page](#)[Abstract](#)[Introduction](#)[Conclusions](#)[References](#)[Tables](#)[Figures](#)[◀](#)[▶](#)[◀](#)[▶](#)[Back](#)[Close](#)[Full Screen / Esc](#)[Printer-friendly Version](#)[Interactive Discussion](#)

Initial fate of fine ash

U. Niemeier et al.

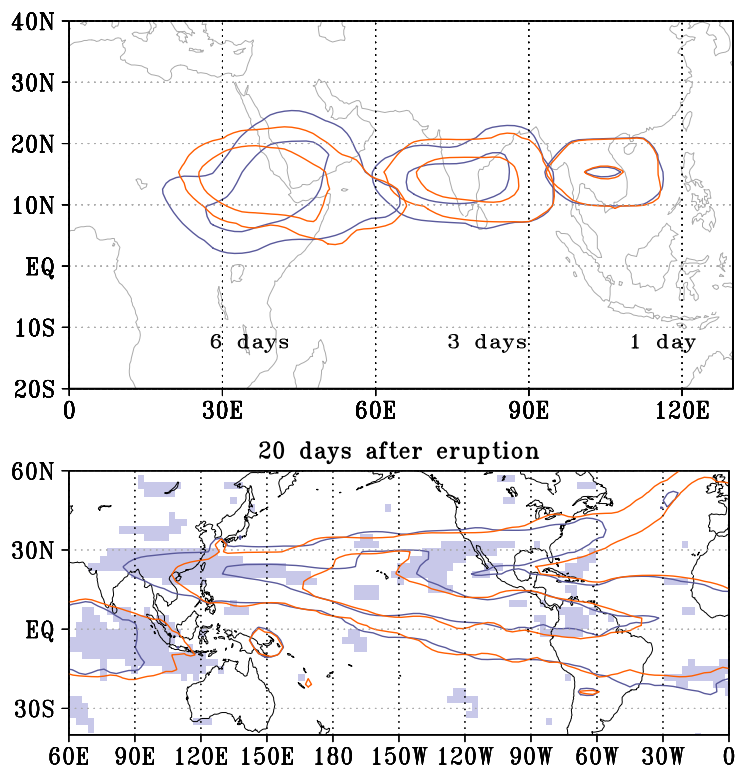


Fig. 9. Distribution of sulfur burden ($\text{SO}_2 + \text{SO}_4^{2-}$) in a simulation excluding (orange) and including (blue) fine volcanic ash (Pt1_ens). Top: Sulfur at 12:00 GMT one, three and six days after the eruption. The outer concentration line represents $2.5 \times 10^{-4} \text{ kg(S)/m}^2$, the inner line has different concentrations on the different days, to mark the position of the cloud maximum. Bottom: Distribution of sulfur twenty days after the eruption. The outer concentration line represents $5 \times 10^{-6} \text{ kg(S)/m}^2$. Areas shaded grey denote significance levels above 99%.

[Title Page](#)[Abstract](#)[Introduction](#)[Conclusions](#)[References](#)[Tables](#)[Figures](#)[◀](#)[▶](#)[◀](#)[▶](#)[Back](#)[Close](#)[Full Screen / Esc](#)[Printer-friendly Version](#)[Interactive Discussion](#)

Initial fate of fine ash

U. Niemeier et al.

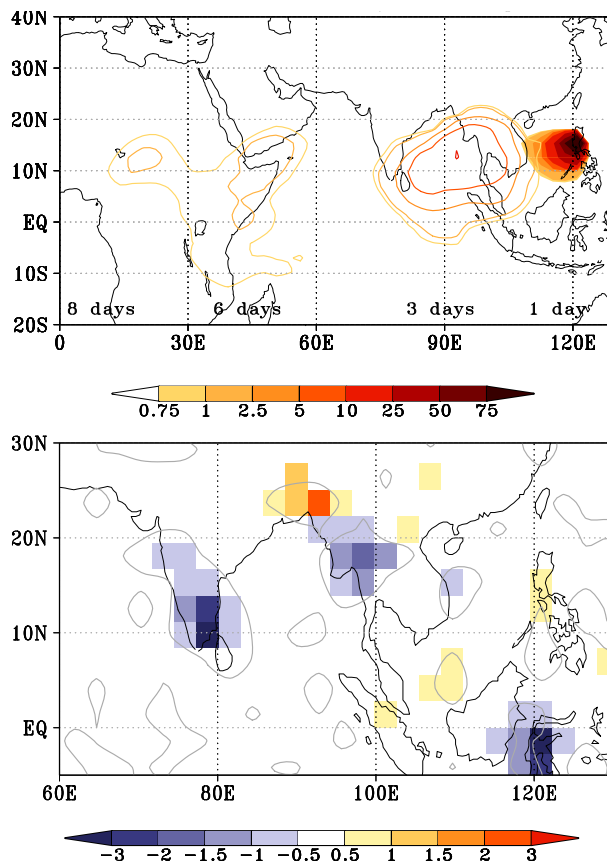


Fig. 10. Development of the aerosol optical depth of fine ash over the first week after the Mt Pinatubo eruption (top) and differences in the 2-m-temperature [K] comparing the simulation with and without ash (bottom) (Case Pt10_ens). Grey lines give 99% significance level.

[Title Page](#)[Abstract](#)[Introduction](#)[Conclusions](#)[References](#)[Tables](#)[Figures](#)[◀](#)[▶](#)[◀](#)[▶](#)[Back](#)[Close](#)[Full Screen / Esc](#)[Printer-friendly Version](#)[Interactive Discussion](#)

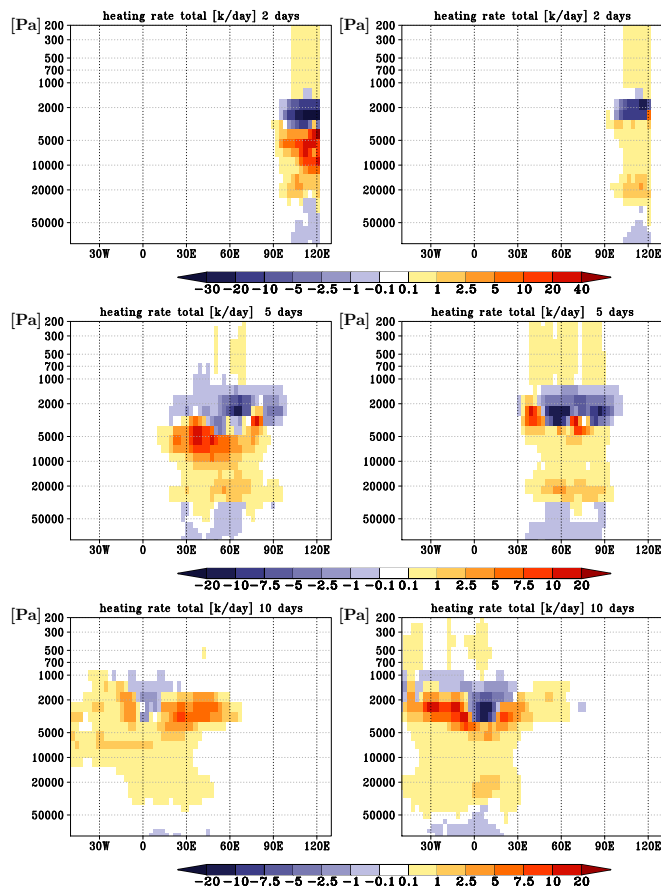


Fig. 11. Heating rates [K/day] two days (top), five days (middle), and ten days (bottom) after the eruption in a simulation including ash (left) and without ash (right) (Pt10_ens). Given is a vertical cross section along 15° N and [Pa] as vertical coordinate.

[Title Page](#)[Abstract](#)[Introduction](#)[Conclusions](#)[References](#)[Tables](#)[Figures](#)[◀](#)[▶](#)[◀](#)[▶](#)[Back](#)[Close](#)[Full Screen / Esc](#)[Printer-friendly Version](#)[Interactive Discussion](#)

Initial fate of fine ash

U. Niemeier et al.

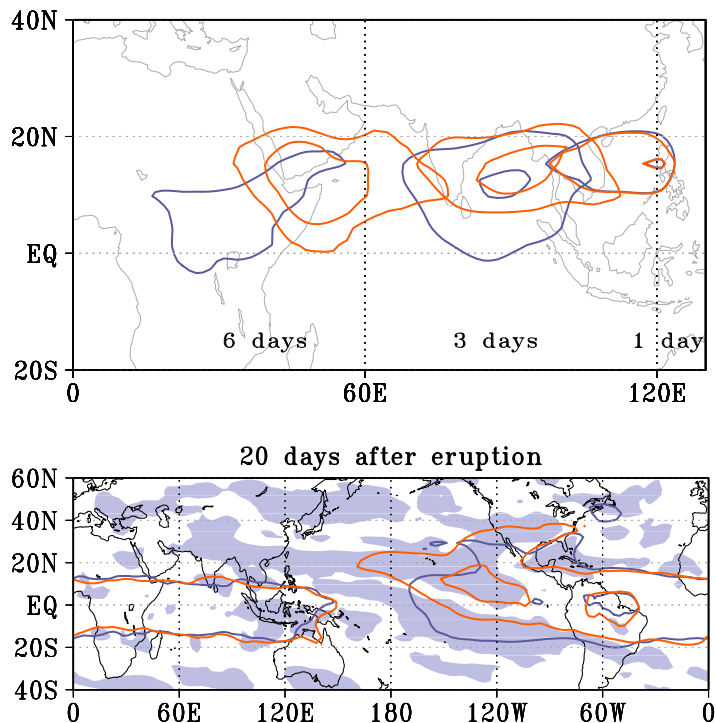


Fig. 12. Distribution of sulfur burden ($\text{SO}_2 + \text{SO}_4^{2-}$) in a simulation excluding (orange) and including (blue) fine volcanic ash (Ptl_{ens}). Top: Sulfur at 12:00 GMT one, three and six days after the eruption. The outer concentration line represents $4 \times 10^{-3} \text{ kg(S)/m}^2$, the inner one has different concentrations on the different days, to mark the position of the cloud maximum. Differences are significant. Bottom: The distribution of sulfur twenty days after the eruption. The outer concentration line represents $2 \times 10^{-4} \text{ kg(S)/m}^2$. Differences are significant in the grey shaded areas.

[Title Page](#)
[Abstract](#)
[Introduction](#)
[Conclusions](#)
[References](#)
[Tables](#)
[Figures](#)
[◀](#)
[▶](#)
[◀](#)
[▶](#)
[Back](#)
[Close](#)
[Full Screen / Esc](#)
[Printer-friendly Version](#)
[Interactive Discussion](#)


Initial fate of fine ash

U. Niemeier et al.

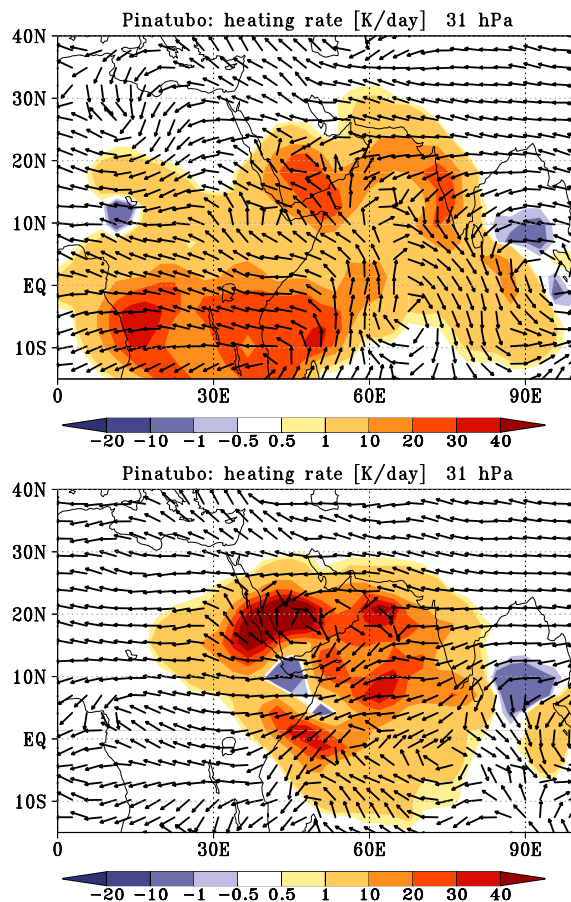


Fig. 13. Wind pattern and heating rates [K/day] at 31 hPa in the simulation containing ash (top) and without ash (bottom) (Pt10_ens).

[Title Page](#)[Abstract](#)[Introduction](#)[Conclusions](#)[References](#)[Tables](#)[Figures](#)[◀](#)[▶](#)[◀](#)[▶](#)[Back](#)[Close](#)[Full Screen / Esc](#)[Printer-friendly Version](#)[Interactive Discussion](#)

Initial fate of fine ash

U. Niemeier et al.

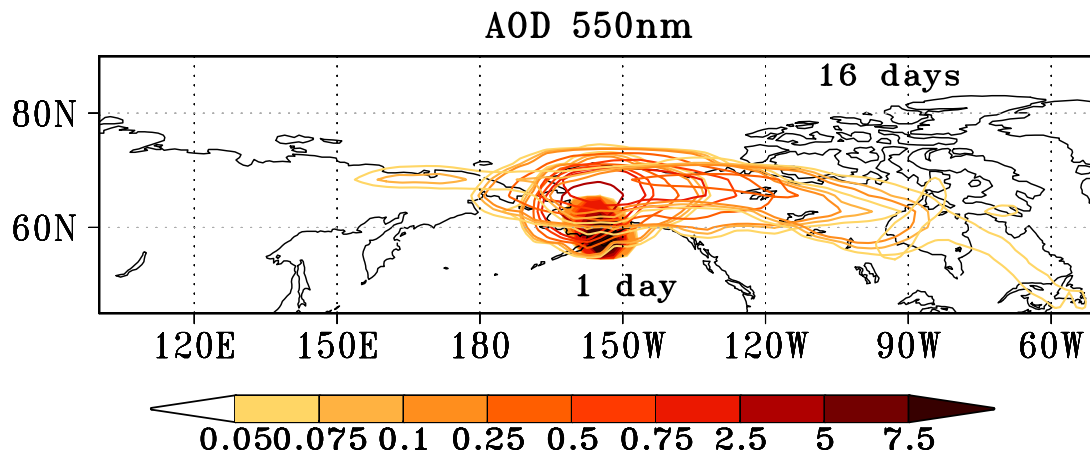


Fig. 14. Development of the aerosol optical depth of fine ash over the first week after the eruption at Mt. Katmai (Case Kat1_ens).

[Title Page](#)[Abstract](#)[Introduction](#)[Conclusions](#)[References](#)[Tables](#)[Figures](#)[◀](#)[▶](#)[◀](#)[▶](#)[Back](#)[Close](#)[Full Screen / Esc](#)[Printer-friendly Version](#)[Interactive Discussion](#)

Initial fate of fine ash

U. Niemeier et al.

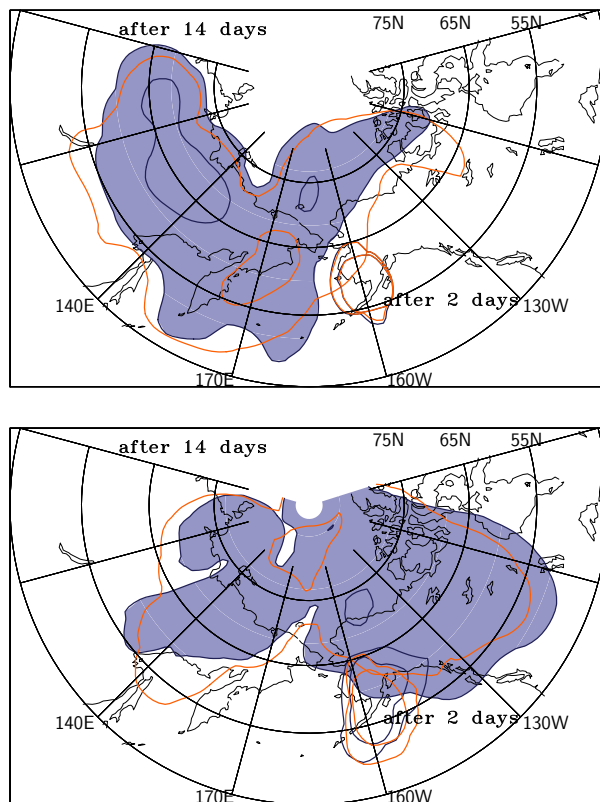


Fig. 15. Distribution of sulfur burden ($\text{SO}_2 + \text{SO}_4^{2-}$) two and 14 days after the eruption in a simulation excluding (orange) and including (blue) fine volcanic ash as mean of a five simulations ensemble. The outer concentration line represents $0.0001 \text{ kg(S)}/\text{m}^2$, the inner line $0.001 \text{ kg(S)}/\text{m}^2$. Top: Eruption at 1st of June (Kat1_ens). Bottom: Eruption at 5th of June (Kat1-5).

[Title Page](#)[Abstract](#)[Introduction](#)[Conclusions](#)[References](#)[Tables](#)[Figures](#)[◀](#)[▶](#)[◀](#)[▶](#)[Back](#)[Close](#)[Full Screen / Esc](#)[Printer-friendly Version](#)[Interactive Discussion](#)

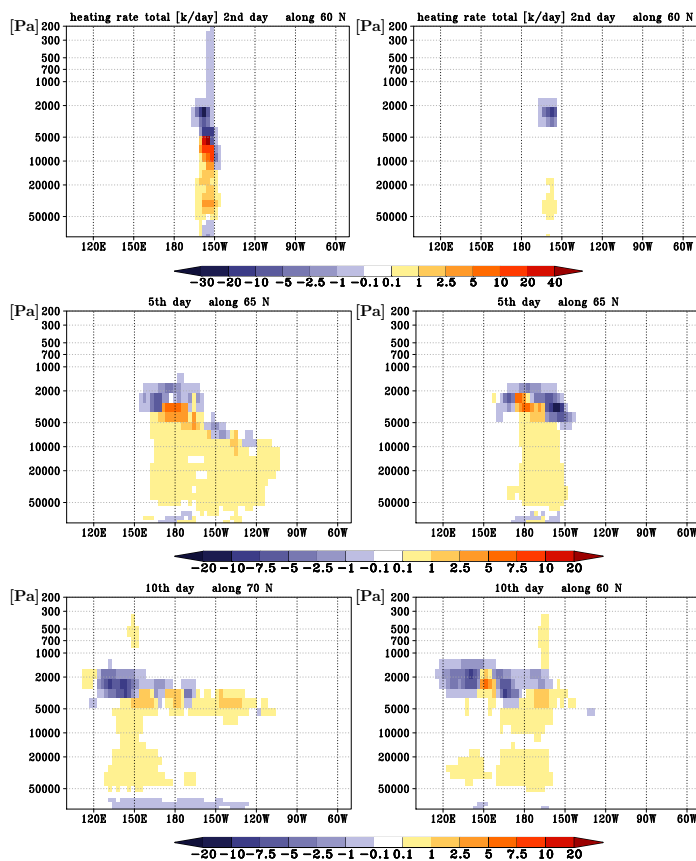


Fig. 16. Total heating rates [K/day] as a daily mean two days (top), five days (middle), and ten days (bottom) after the Mt. Katmai eruption (Kat1_ens) in a simulation including ash (left) and without ash (right). Given is a vertical cross section along different latitudes where the maximum concentration is located.

[Title Page](#)[Abstract](#)[Introduction](#)[Conclusions](#)[References](#)[Tables](#)[Figures](#)[◀](#)[▶](#)[◀](#)[▶](#)[Back](#)[Close](#)[Full Screen / Esc](#)[Printer-friendly Version](#)[Interactive Discussion](#)

Initial fate of fine ash

U. Niemeier et al.

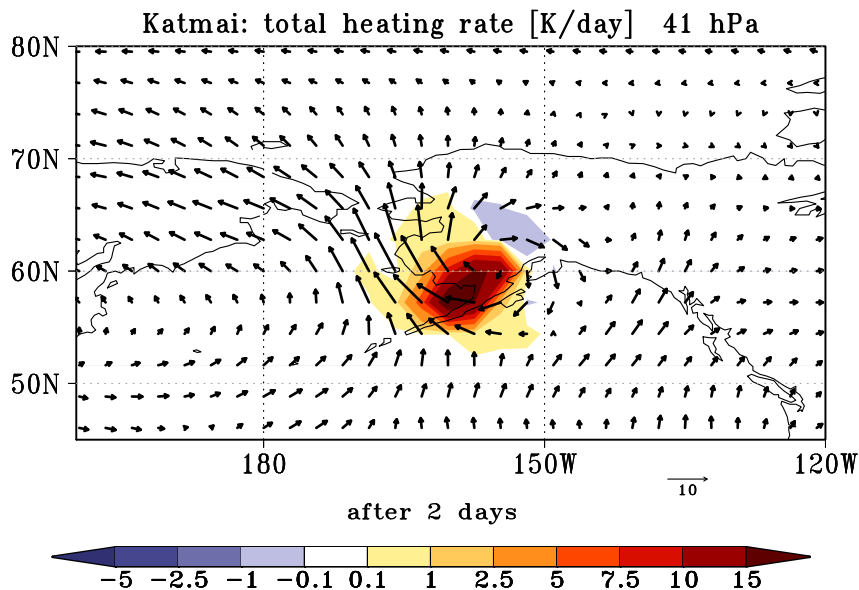


Fig. 17. Radiative heating [K/day] and wind vectors at 41 hPa, 36 h after the eruption showing the rotation of the cloud in the simulation with ash (Kat1_ens).

[Title Page](#)[Abstract](#)[Introduction](#)[Conclusions](#)[References](#)[Tables](#)[Figures](#)[◀](#)[▶](#)[◀](#)[▶](#)[Back](#)[Close](#)[Full Screen / Esc](#)[Printer-friendly Version](#)[Interactive Discussion](#)

Initial fate of fine ash

U. Niemeier et al.

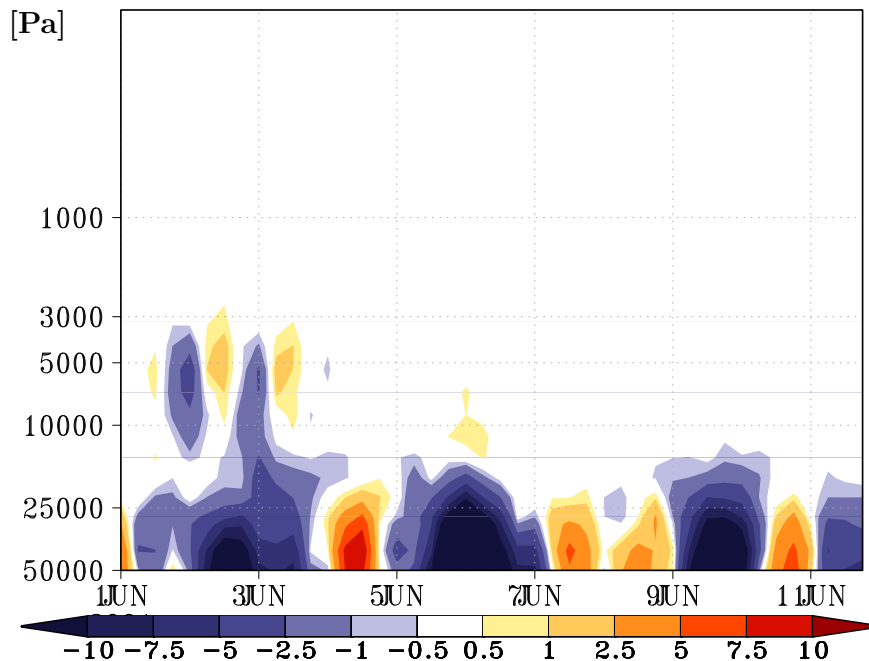


Fig. 18. Development of vertical velocity [$\text{Pa/s} \times 0.01$] over the first days in the volcanic cloud containing sulfate and ash (Kat1_ens).

[Title Page](#)[Abstract](#)[Introduction](#)[Conclusions](#)[References](#)[Tables](#)[Figures](#)[◀](#)[▶](#)[◀](#)[▶](#)[Back](#)[Close](#)[Full Screen / Esc](#)[Printer-friendly Version](#)[Interactive Discussion](#)

Initial fate of fine ash

U. Niemeier et al.

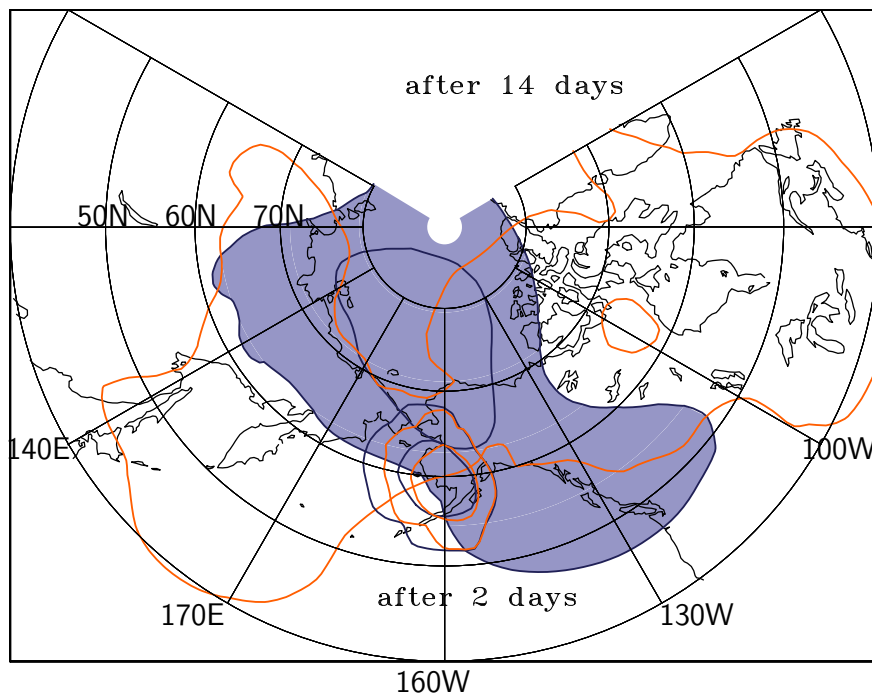


Fig. 19. Distribution of sulfur burden ($\text{SO}_2 + \text{SO}_4^{2-}$) two and 14 days after the eruption in a simulation excluding (orange) and including (blue) volcanic ash (Kat10_ens). The outer concentration line represents 0.001 kg(S)/m^2 .

[Title Page](#)[Abstract](#)[Introduction](#)[Conclusions](#)[References](#)[Tables](#)[Figures](#)[◀](#)[▶](#)[◀](#)[▶](#)[Back](#)[Close](#)[Full Screen / Esc](#)[Printer-friendly Version](#)[Interactive Discussion](#)

Initial fate of fine ash

U. Niemeier et al.

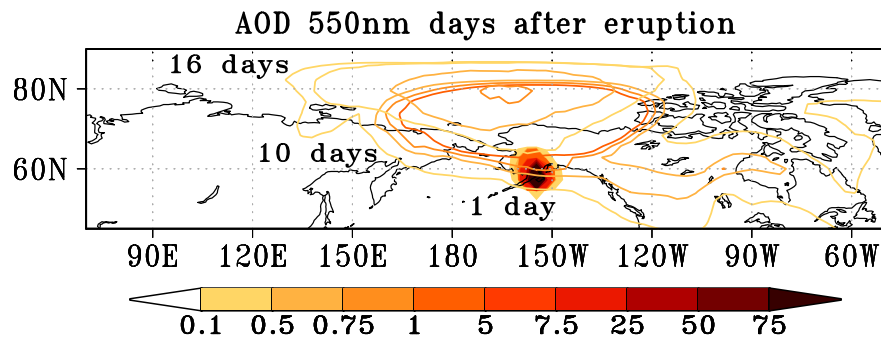


Fig. 20. Aerosol optical depth of fine ash one, 10 and 16 days after the eruption (Kat10.ens).

[Title Page](#)[Abstract](#)[Introduction](#)[Conclusions](#)[References](#)[Tables](#)[Figures](#)[◀](#)[▶](#)[◀](#)[▶](#)[Back](#)[Close](#)[Full Screen / Esc](#)[Printer-friendly Version](#)[Interactive Discussion](#)

Initial fate of fine ash

U. Niemeier et al.

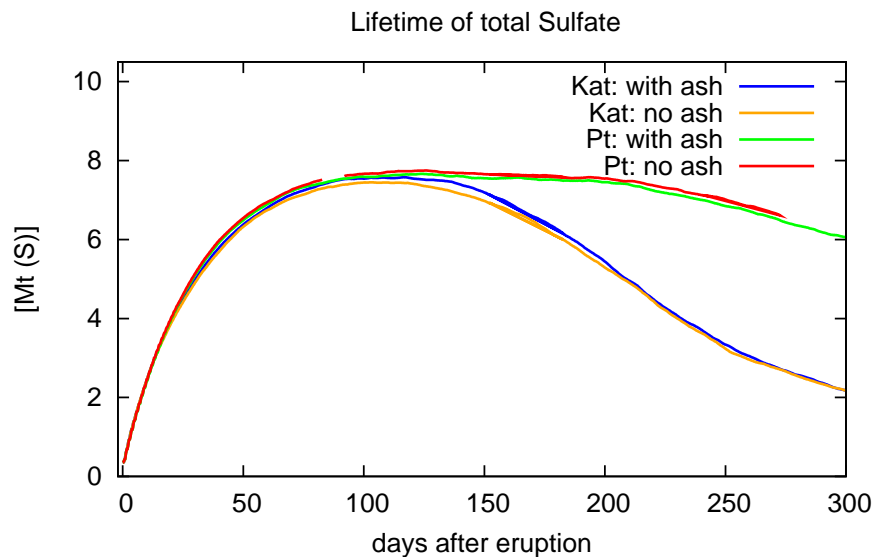


Fig. 21. Global total sulfate concentration kg(S)/kg for 300 days after the eruption in the simulation Pt1 and Kat1.

[Title Page](#)[Abstract](#)[Introduction](#)[Conclusions](#)[References](#)[Tables](#)[Figures](#)[◀](#)[▶](#)[◀](#)[▶](#)[Back](#)[Close](#)[Full Screen / Esc](#)[Printer-friendly Version](#)[Interactive Discussion](#)